Embedded impedance based state-of-charge estimation

CARL BOMAN

KTH Industrial Engineering
and Management

Master of Science Thesis
Stockholm, Sweden 2014

KTH Industrial Engineering and Management

Master of Science Thesis MMK 2014:65 MDA 502

Embedded impedance based state-of-charge estimation

Carl Boman

Approved:	Examiner:	Supervisor:
2014-09-08	Hans Johansson	Mikael Hellgren
	Commissioner:	Contact person:
	Inmotion Technologies AB	Christian Sandberg

Abstract

Estimating the battery state-of-charge is an important aspect of prolonging battery life and optimizing discharge cycles. In this thesis, a hybrid method for estimating state-of-charge for lead-acid batteries is developed and implemented in a motor controller. The method uses a combination of impedance measurements and a linear regression model for estimation. Measurements are done at stand-still. The method does not require sensors that are external to the motor controller or auxiliary battery connections other than terminal connections. The final estimation model shows good results but exhibits a slight ambient temperature dependence.

KTH Industriell teknik
och management

Examensarbete MMK 2014:65 MDA 502

Embedded impedance based state-of-charge estimation

Carl Boman

Approved:	Examiner:	Supervisor:
2014-09-08	Hans Johansson	Mikael Hellgren
	Commissioner:	Contact person:
	Inmotion Technologies AB	Christian Sandberg

Sammanfattning

Att estimera ett batteris laddstatus är av stor vikt när det gäller att förlänga livslängden hos batteriet och att optimera urladdningscykler. I detta examensarbete utvecklades en hybridmetod för laddstatusestimering som sedan implementerades i en motorstyrning. Metoden använder en kombination av impedansmätningar och en linjär regressionsmodell för estimering. Mätningar görs vid stillastående. Metoden kräver inga externa sensorer eller andra batterianslutningar än terminalanslutningarna. Den slutgiltiga modellen uppvisar god prestanda men uppvisar ett visst temperaturberoende.

Acknowledgements

I would like to take the opportunity to thank everyone that have contributed with help, thoughts, support and ideas throughout this thesis.

First, I extend my gratitude to my supervisor Mikael Hellgren not only for being my supervisor but also for helping me with everything concerning KTH, initially introducing me to Christian at Inmotion Technologies and for his enthusiasm. I am also very grateful for my company contact and work site supervisor Christian Sandberg who spent a great deal of time explaining, debugging and not least for offering me the master thesis. Extending beyond Christian, I must thank nearly everyone of his colleagues for their ideas and shown interest.

Last but not least I would like to thank my dear wife Helene who has supported me throughout my engineering studies and kept me from taking it too easy.

Contents

Nomenclature and abbreviations

Notations

p	Peukert exponent.
R	Battery hour rating, in hours.
ϕ	Phase offset between current and voltage waves, in system ticks.
R_i	Measured Ohmic impedance, in Ohms.
V_t	Battery terminal voltage, in Volts.
$\dot{V}_t$	$\frac{d}{dt}V_t$, in V/s.

Abbreviations

EV Electric vehicle.

Li-ion Lithium-ion.

NiMH Nickel metal hydride.

SOC State of charge.

SOH State of health.

Ah Ampere-hour.

OCV Open circuit voltage.

CCA Cold cranking amps, in Amperes.

IDE Integrated development environment

CAN Controller area network

PWM Pulse width modulation

Chapter 1

Introduction

In this day and age we are highly dependent on energy in many ways. We need it to power devices that provide us with everything from heat to cold to transportation and communication. The general migration to wireless systems has caused a boom in battery technology, pushing more energy dense alternatives such as Li–Ion and NiMH forward. Commonly noted advantages except the higher energy density includes lower battery weight and the utilization of more environmentally friendly materials. However, the newer technologies come at a higher cost per kWh and requires more complex infrastructure such as battery management systems to supervise cell aging and charging/discharging.

One battery consuming market segment stands out from most others, namely the materials handling and low cost electric vehicle market. In materials handling, low battery weight is more of a disadvantage than an advantage since it is used to counter-balance the handled material, and the low cost and simple infrastructure of the lead acid battery technology makes a shift to newer types hard to motivate.

Inmotion Technologies AB is a company that designs and manufactures a variety of products in the controls area, with emphasis on hybrid or all-electric vehicle control. The main end sector is materials handling. The Stockholm office houses R&D, manufacturing, quality and testing, applications engineering and sales.

1.1 Background

Although considered rugged and insensitive to deep cycling, neglectful use of lead acid batteries can shorten its life span significantly. It is important to not discharge the battery too deeply, and also to not store it while discharged. This damages the battery which is very costly for the owner, and also generates large amounts of lead waste. The easiest way to avoid this is to monitor the state of charge (SOC) and recharge the battery if needed. The problem is that precise SOC measurement is hard and usually involves external hardware. Specifically in vehicle lead acid applications, the battery is often disconnected from the vehicle while charging. This makes the amount of charge supplied to the battery ”invisible” to vehicle mounted

monitors that track current input/output dynamics. It would be preferable to do the measurement without external sensors or hardware to reduce complexity, and also to do estimates of absolute SOC instead of using a relative method of tracking input/output currents to avoid drifting.

The reason as to why we aren't already seeing such minimalistic SOC estimators is because of the fact that batteries are inherently non-linear. They need advanced models to be accurately approximated, alternatively be tested in a controlled laboratory environment in order to determine the exact SOC. Simple hardware SOC monitors are being sold today, but most rely on terminal voltage and look-up tables to estimate SOC and that approach is highly sensitive to ambient temperature, time since last load application, and the state of health (SOH) of the battery. Inmotion Technologies AB has requested an investigation into the development of a SOC estimation algorithm to be embedded in their motor controllers. This thesis work is initially intended for powered pallet trucks and stackers which might benefit from low-cost and low-complexity SOC estimation functionality.

1.2 Hypothesis

With sufficiently advanced motor control, an accurate SOC estimation algorithm can be designed and implemented without using external sensors.

Grounds for accepting the hypothesis

To accept the hypothesis, the SOC estimation algorithm should be able to offer a performance within ± 10 percentage units in the final prototype, not depend on any external sensors and be able to execute in the ambient processor environment.

1.3 Purpose

The purpose of this thesis is to develop a novel minimalistic approach for embedded SOC estimation.

1.4 Scope

The scope of this thesis is:

- Set up a laboratory environment for battery applications.
- Identify possible methods of estimation for the target application.
- Design an embedded SOC estimation algorithm implemented in a motor controller based on most suitable method.
- Perform validation/verification and estimate the accuracy of the algorithm.

- Ensure that the estimation function fits in the embedded environment without exclusion of any existing functionality.

1.5 Delimitations

- Estimation must be performed without using external sensors and/or hardware except for in the development phase.
- Due to scope size, this thesis will not cover:
  - ambient climate dependencies, it would expand the scope beyond what is reasonable.
  - effects of battery health, since there is only access to a single battery.
  - behavioral differences between batteries, inverters and/or motors, due to scope.
  - vehicle implementation and field testing, due to scope and lack of a vehicle for testing.
  - on-line SOC estimation – meaning during movement and/or operation. This is due to the increased scope and complexity.

1.6 Methodology

This thesis has a deductive approach, data collection was done experimentally and analysis done statistically. Firstly, methods of SOC estimation were collected. Some of these were then iteratively removed from the list of possible implementations after considering constraints such as complexity, software size or dependency on external sensors. The most suitable method was chosen and the subsequent work reflects that choice. Much of the work involved was building a solid foundation of measurable data for parameterization.

Thesis strategy

Initially, a background study is performed to identify methods of estimation. These methods are then evaluated based on complexity, calculation times and flexibility. The methods that are assumed to be implementable are then ranked and possibly combined to form the final estimation model.

1.7 Report outline

Frame of reference

Covers the theoretical background needed for understanding the details of the problem and implementation.

Lab setup

Describes the software and hardware setup that was used.

Method

Details the chosen method of estimation and design decisions.

Implementation

Explains design choices and software architecture.

Results

This section contains an account of results.

Analysis and conclusion

Analysis of the results and final words on the hypothesis of the thesis.

Future work

Possible future extensions to the work in this thesis.

Chapter 2

Frame of reference

2.1 Lead acid batteries

This section describes the history, construction and characteristics of the lead acid battery.

2.1.1 Battery overview

The lead acid battery was invented in 1859 by a French physicist, Gaston Planté. It is – in its essence – a number of lead and lead oxide plates submerged in sulfuric acid electrolyte, with separators in between. There are two general lead acid battery types, namely the ”starting battery” and the ”deep cycle battery”. Both are constructed roughly the same way, with minor variations pertaining to the different characteristics and applications. This is described in more detail in section 2.1.3.

2.1.2 General principle of operation

A fully charged lead acid battery cell consists of a negative plate of lead and a positive plate of lead oxide submerged in sulfuric acid. As the cell discharges, both plates react with the electrolyte and form lead sulfate. The electrolyte in turn is gradually diluted to water by the recombination of aqueous hydrogen and oxygen. The process is reversed during charging.[1]

Lead acid cell reaction

$$PbO_2 + Pb + 2H_2SO_4 \underset{\textbf{Charge}}{\overset{\textbf{Discharge}}{\rightleftarrows}} 2PbSO_4 + 2H_2O$$

2.1.3 General characteristics and behavior

Lead acid type batteries are relatively insensitive to over charging and over discharging compared to for example lithium ion type batteries, making it a safer

choice for consumer applications. Deep cycle lead acid batteries are designed to power devices such as electric motors with a medium continuous current draw for longer periods of time, as opposed to the starting battery. The starting battery is designed to provide very high currents while powering the starter motor in a combustible fuel vehicle, after which it is float charged by the generator and providing a limited current to various electrical systems. The major difference in construction between the two is the surface area of the plates compared to the overall plate mass. A larger surface area can provide higher currents due to an electrochemical phenomenon called *surface charge*, also referred to as *charge diffusion* or *interface charge*. During discharge, current originates from the boundary layer of the electrodes and electrolyte. As current is initially drawn from the plate, the surface charge of the plate is "spent", and further current draw must rely on the rate of charge diffusion from the inner volume of the electrode to the surface. This causes a current drop after the initial surge. It can also cause a reduction in charge acceptance when charging with a constant current, as the charge accumulates near the surface and thereby decreases the voltage differential at the boundary layer.[2]

Factors affecting battery health

Another phenomenon that also causes drops in maximum current output is *stratification*. Stratification is an electrolyte gradient from acid to water that may appear either during high rates of discharge or after several charge/discharge cycles where the lighter water gathers at the top of the battery and the heavier acid at the bottom. This causes an uneven potential distribution over the plate surface that also gives an illusion of a higher state of charge by showing a "false" low internal resistance. This can also have negative effects on long-term battery health. The water that gathers at the top of the cells causes corrosion, while the bottom is the only area in contact with the denser electrolyte and providing a current. The bottom part is then more deeply cycled and more often deeply discharged, which may cause *sulfation*. Lead sulphate is always formed on the surface of the active material during discharge and normally easily reverts to lead and lead oxide, but after long and deep discharging the lead sulphate can become crystalline. In this state the cell will not accept charge as easily, it might start to shed its active material and the crystal formation might put the cell structure under mechanical stress.[3][4]

2.1.4 Capacity and its dependencies

Coulombic efficiency

As with all batteries, there are several factors that affect the total capacity. Due to the non-linear behavior of the battery, capacity is expressed in Ampere hours (Ah) at a predetermined discharge rate, and also generally at a specific temperature. The rate is called C, and 1 C refers to the current that will theoretically drain the battery in one hour. For example, a 100 Ah battery has a 1C rate of 100 A. It is important to know the discharge rate for the associated capacity, since a higher

current than specified will have adverse affects on capacity. A German scientist, Wolfgang Peukert, addressed this by introducing an exponent that exponentially increases capacity drain with increasing current. This is used in practice as an extended form of Coulomb counting, and is covered in section 2.2.[5]

Temperature

Temperature is a factor that affects both battery capacity, performance and health. A high temperature increases capacity and performance, but has adverse affects on battery life. Low temperatures does the opposite, and low temperature storage also reduces self-discharge due to the decreased performance. The temperature dependency comes from the need of a certain activation energy dependent on the type of cell reaction. Low temperature also slows electrolyte convection which is the cause of reduced cold cranking amps (CCA), which is the maximum current output from a "cold" state. In this context, "cold" means a battery that has been at rest and is at ambient temperature.[6][7]

Electrolyte density

There are two main factors affecting electrolyte density: temperature and concentration of sulfuric acid. A decrease in density can be ascribed to either decreased acid concentration or increased temperature. In the case of concentration decrease, this would affect SOC in a negative way due to loss of charge transfer ions. If the cause of density decrease would be an increase in temperature, the effect on SOC would be positive due to increased available activation energy and electrolyte convection speed. It is important to consider these phenomena when doing analysis of data containing temperature and/or electrolyte density.[8][9]

Coup de Fouet

Another phenomenon that adds additional complexity to SOC estimation is the so called *coup de fouet* (lit. "crack of the whip") which is a phenomenon that occurs at the first time interval of discharge when the battery is fully charged. The *coup de fouet* can be observed as a sudden initial terminal voltage drop, that after a relatively short time – dependent on capacity and discharge current – displays a local minimum (the "trough" voltage) and then starts to increase to a local maximum (the "plateau" voltage). See figure 2.1. Not much research has been done to determine the mechanism of the phenomenon, but there is an explanation that is said to be widely accepted in literature. According to that explanation, the responsible mechanism is a crystallization overvoltage, an energy gap necessary for lead sulphate formation. [10][11]

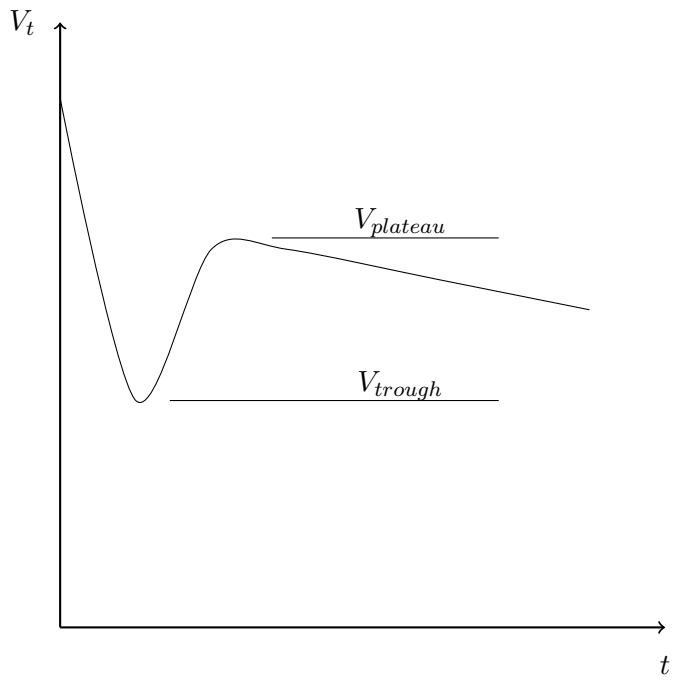

Figure 2.1: Typical behavior of the *coup de fouet*

2.1.5 Modeling

There is a large number of models for lead acid batteries, all increasing in complexity with the demand for accuracy. Major model types are chemical, machine learning and equivalent circuit models. Each type has its advantages and disadvantages, and is chosen depending on the type of application. One of the most common simpler models is the Randles model, as seen in figure 2.2.[12]

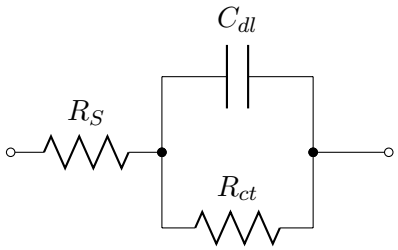

Figure 2.2: Basic Randles battery model

In the figure, R_S denotes active electrolyte resistance, C_{dl} the double layer capacitance of the battery and R_{ct} the charge transfer resistance. Double layer capacitance is a result of the electrode being immersed in electrolyte, and charge transfer resistance is ascribed to electrolyte temperature and reaction product concentration among others. [13]

2.2 SOC estimation methods

There are several methods of SOC estimation, and not all are implementable in this thesis work. [14] The methods that have been considered are those that survive the constraints of computational power, program size and ease of implementation. Those that have been considered plausible for implementation are outlined in the running text below.

2.2.1 Impedance measurements

Impedance spectrometry is a general term of measuring impedance at one or more frequencies. The method is common for evaluating electrochemical processes that affect both state of charge and state of health. It is often used to parameterize an equivalent circuit model of the battery, where individual parameters can be correlated to SOH. By analyzing AC frequency response, various relations to SOC have been found.[15]

The method has been said to be quite temperature dependent, although the dependency has been proved to be significantly smaller at frequencies at or above 100 Hz. [16][17]

2.2.2 Coulomb counting

Considered the most common method of estimation, Coulomb counting works by accumulating charge and discharge currents, thereby giving an idea of SOC. The main issue with Coulomb counting is that the Coulombic efficiency is quite different between charge and discharge, charge being less efficient than discharge. This needs to be taken into account in applications that feeds current back into the battery when for example braking. It is also a relative estimator. It does not give an exact value of the state of charge, but only a relative value change from the last known value.[14]
A common way to implement the method with a Peukert modification is

$$SOC = 1 - \frac{1}{C}\int_0^t I(t)^p \mathrm{d}t \tag{2.1}$$

or in discrete form:

$$SOC = 1 - \frac{T}{C}\sum_{i=1}^{n} {I_i}^p \tag{2.2}$$

where C denotes the rated capacity of the battery, p the Peukert exponent – which is usually a value between 1 and 2 – and T the timing period.

2.2.3 Linear model

Attempts have been made to linearize the SOC measurements using various linear models. Usually, parameters depending on the type of application are chosen for estimation and parameters are then established using least-mean-square calculations on an overdetermined linear system, for example using Gaussian or Gauss-Jordan elimination. [14][18]

2.3 Induction motor current control

In the case of three phase AC induction motors, control can be quite complex. This is much attributed to the stationary reference frame and rotating magnetic fields involved in torque production. Induction motors work by the stator magnetic field inducing a rotor current and in turn a rotor magnetic field. The rotor magnetic field opposes the stator field, and so the rotor starts to turn in the same direction as the stator field. Under load, the rotor will rotate at a speed somewhat below synchronous speed, which is the stator field speed. Because the rotor current is induced by the change in the magnetic field, if the rotor rotates at synchronous speed there is no current induced.

To reduce complexity, it is possible to transform the three phase stationary reference frame to a rotating frame of DC quantities using a so called dq0-transform. The transform is in essence a series of stationary rotations and applying a rotation with the speed of the rotating stator field. The result is two orthogonal axes, the direct and the quadrature axis. The direct axis is involved in flux linkage and the direct axis current is also called the magnetization current. The quadrature axis current is responsible for motor torque production and is in quadrature to the direct axis. Operations on the currents can then be done in the dq-plane and subsequently inversely transformed back to the three phase stationary reference frame. [19]

This thesis work is only concerned with the direct axis current as the goal is to not produce torque.

Chapter 3

Laboratory environment

3.1 Environment schematic

The following figure represents the experimental setup used in the lab. The major components are descried in text in the following sections.

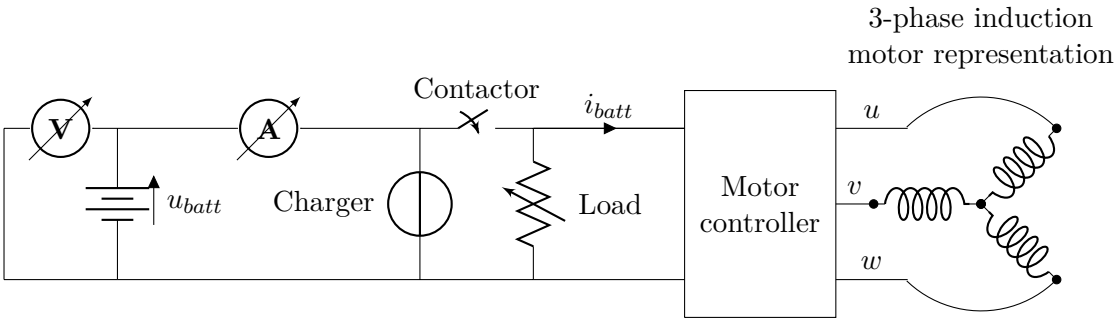

Figure 3.1: Laboratory environment schematic. Only the battery, motor controller and motor would be present in a live application.

3.2 Battery

The battery used in this thesis work is a 24 Volt Hawker-Enersys Perfect Plus rated 120 Ah when discharging at a 5 hour rate. This means that the battery is to be considered ”depleted” after a 5 hour discharge at 24 A. The effective SOC at depletion is 20%, to protect the battery from being over-discharged.[8]

3.2.1 Battery selection and acquisition

With the help of Inmotion Technologies AB contact was made with the battery supplier of one of the company’s bigger clients. After consulting with a salesman at Enersys-Hawker, a 24 V, 120 Ah battery with a central water refill system was

ordered. The capacity was determined by the fact that there would be extensive cycling of the battery during the thesis work, and charging/discharging a larger battery would take too much time.

3.3 Current transducer

For current measurements, a IT 700-S current transducer was used. The transducer was mounted so that it captured both charge and discharge currents. The transducer outputs a voltage that is translated to the actual measured current by a factor of 1750. The voltage output was fed to and translated into current by the DAQ described in section 3.4.

3.4 Data acquisition

In order to log and supervise system voltage and currents, a Dewesoft Dewe-43 DAQ was wired to the battery terminals and to the current sensor. It was used to verify the DC current regulation done by the motor controller, with respect to amplitude, frequency and DC offset.

3.5 DC load unit

To discharge the battery without potentially overheating the motor used in SOC estimation, a Chroma 63203 DC load was connected to the battery. It provided constant current discharge for cycling.

3.6 Motor controller

The motor controller used was a Gen6 ACS36S. The controller can be seen as a 24 V DC to 3-phase AC inverter with variable amplitude and frequency.

3.7 Density meter

To be able to measure the density of the electrolyte, a mechanical floater type Biltema density meter was rebuilt to work with the battery. It measures densities between roughly 1100 to 1350 g/l which works well for this application.

3.8 Software

This section describes the software development environment.

Figure 3.2: Gen6 ACS36S. Source: Inmotion Technologies AB

3.8.1 IDE

Software development was primarily done in Visual Studio. Even though development could have been done with any text editor, the code completion functionality was very efficient when working on a large software platform.

3.8.2 Compilation and code download

The build system was simple enough to not integrate into Visual Studio. Code compilation was done with the IAR compiler and download to the motor controller was done over CAN with the software CodeLoader. CAN is a well known serial communications bus. [20]

3.8.3 On-line parameter adjustment

To make adjustments to the software parameters while running the application in the motor controller, the locally developed PC software DriveTool was used. DriveTool communicates over the CAN bus with the motor controller. The controller has a communications layer that can externalize selected application variables. Those variables can then be adjusted and visualized directly in the DriveTool environment in text form or in bar sliders or gauges.

Chapter 4

Method

This thesis work is divided into several distinct parts. Those parts are described in detail in this section.

4.1 Data acquisition

First, data was collected to provide a basis for validation and verification of SOC estimation. This was done by battery discharge from 100 to 20% with continuous density measurements. Electrolyte density has a linear relationship with SOC, which is why this method was chosen. [14]

Measurements were indeed linear over time with a constant current draw, and a simple conversion from electrolyte density to SOC was formed:

$$SOC = 0.5 \cdot \rho_{electrolyte} - 550 \tag{4.1}$$

which puts a 100% SOC at 1300 g/l, and 20% at 1140 g/l as per the battery data sheet, ρ denoting the density in g/l.

Figure 4.1 shows the linear relationship between measured electrolyte density and calculated SOC. The battery was discharged at the rated current of 24 A for 5 hours, giving the rated capacity of 120 Ah. This was later used throughout the thesis work to verify prototype estimation algorithms and for providing a regression target.

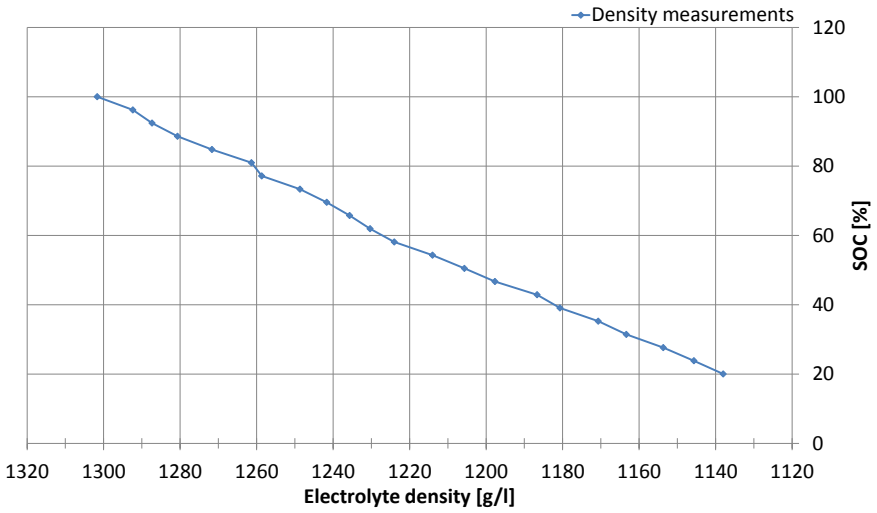

Figure 4.1: Plot over electrolyte density versus SOC

4.2 Method of SOC estimation

The chosen estimation method is mainly based on impedance measurements but also incorporates a linear model for regression. Impedance measurements make up the data foundation used for estimation with the help of linear regression. This was mainly decided because of the versatility of the impedance method and the fact that there was no need for a battery model other than for supporting intuition when doing data analysis. In addition, a linear model that can be externally parameterized shrinks the application footprint compared to more complex embedded implementations. A downside with the method is that measurements cannot be taken while there is a load present, making it a requirement that the vehicle is at stand still with a minimal amount of external loads. With the constraint of not using external sensors, the chosen combination was perceived to offer the greatest flexibility and ease of implementation. Implementation is described in section 5.6.

4.3 DC bus current control

To excite a sine wave on the DC bus, it was necessary to control the voltages and currents on the AC side (or motor side) of the system. DC bus voltage, direct and quadrature voltages and currents are measured by the motor controller. DC bus current is derived from those values. To control the DC bus current, stepwise updates of the voltage reference on the AC side were made using the following power relationship:

$$\begin{aligned} P_{batt} \approxeq P_{AC} \xrightarrow{\mathcal{T}_{dq0}} P_{batt} &\approxeq P_d + P_q \\ u_{batt} i_{batt} &\approxeq \frac{3}{2}(u_d i_d + u_q i_q) \end{aligned} \tag{4.2}$$

Where P_x denotes power in Watts and u_x and i_x momentary voltage and current, respectively. Since measurements are not done parallel in time, there is a slight time delay between them. The fraction $\frac{3}{2}$ comes from the equation of instantaneous power for a $dq0$–transformed quantity.[19] This delay is hard to define, but can be assumed to be of minor importance since the regulation period is much smaller than the regulated wave form period, and the *total* run time of the estimation function is a few µs. Equation 4.2 is said to be an approximate equality since u_d and u_q are not measured but calculated from DC bus voltage and PWM duty cycle. The built-in sensors measure DC voltage and AC currents in two phases. In this application, the accuracy in this calculation is not of great importance as long as the current is in the form of a proper sine wave on the DC bus.

Since we want the rotor to be stationary during the estimation we excite the current by stator losses only, therefore $u_q = 0$ and equation 4.2 becomes

$$u_{batt} i_{batt} = \frac{3}{2} u_d i_d \tag{4.3}$$

Internally, a discretized sine wave current reference was kept using amplitude, DC offset and frequency parameters. The current reference is updated at 4 kHz, which is the period of the SOC estimation algorithm. The momentary amplitude of the reference is

$$i_{battref} = V_{offset} + A \cdot \sin 2\pi ft \tag{4.4}$$

where V_{offset} denotes the DC voltage offset, A the sine wave amplitude and f the frequency. The sign of the current had to be kept positive, and in this application this means in the direction away from the battery. The motor cannot excite a negative current from a state of rest, therefore the current must be kept positive with some margin to avoid dead band effects. The equation becomes

$$i_{battref} = \frac{5A}{4} + A \cdot \sin 2\pi ft \tag{4.5}$$

We now need to translate our DC bus current reference to a reference that the motor controller can use. In this application, the direct axis voltage was used as a reference. Using equation 4.3 gives

$$u_{dref} = \frac{2}{3} \cdot u_{batt} \cdot \frac{i_{battref}}{i_d} \tag{4.6}$$

Validating the current control algorithm was done by data recording with the DAQ unit described in section 3.4. Amplitudes and frequencies were verified with the software scope feature in a PC environment. A reference update at 4 kHz implies that high sine wave frequencies are more prone to generate harmonics which might disturb the estimation process. At the same time, to avoid too much temperature dependency the frequency should be at or above 100 Hz, as explained earlier. As a compromise, a frequency of 150 Hz was chosen. At this frequency, the number of algorithm periods per wave period is

$$\frac{4000s^{-1}}{150s^{-1}} = 26.666\ldots \approx 27 \tag{4.7}$$

and with 27 steps per period a wave of sufficiently good quality can theoretically be excited, as can be seen in figure 4.2.

4.4 Estimation

The method of estimation is actually a hybrid between impedance measurement and a linear model using several different measurements. It consists by 1 second constant current preload draw at several tens of Amperes and 2 seconds of impedance measurements, see figure 4.3. Estimation is performed when the system is approximately equivalent to open circuit. This means shortly after the vehicle has come to a stand still. Note specifically that the system state for estimation is open circuit, and not necessarily at the open circuit *voltage*.

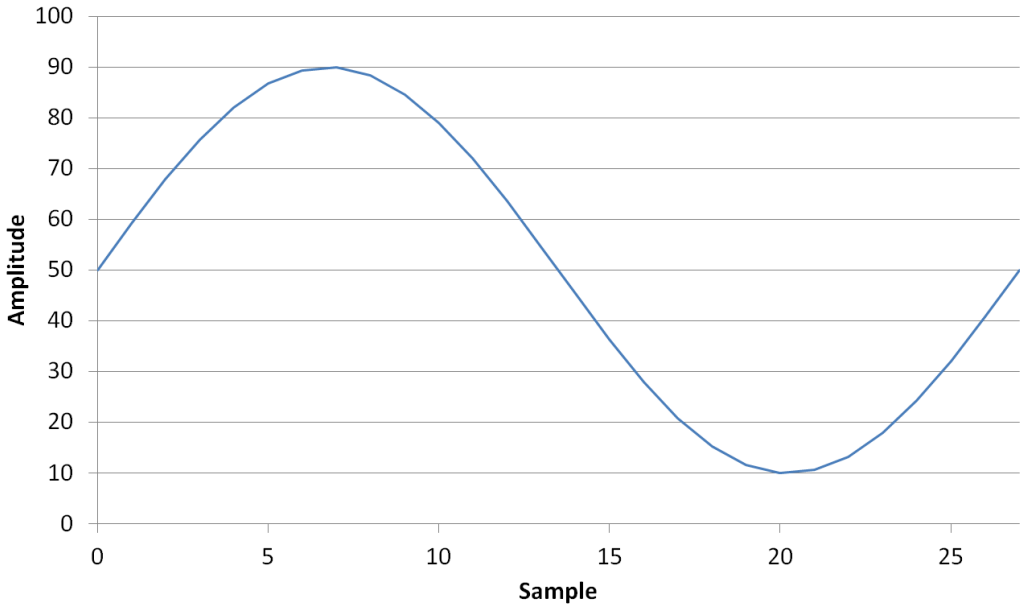

Figure 4.2: Sine wave discretization at 150 Hz

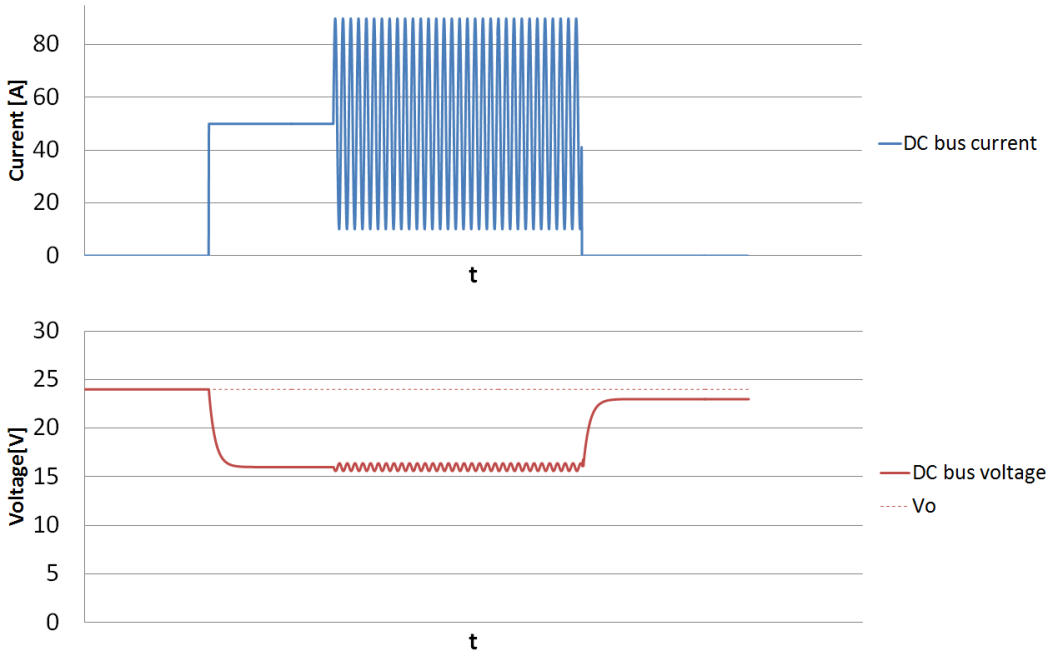

Figure 4.3: Current excitation concept. The dashed line represents the initial terminal voltage and shows the exaggerated difference between voltages before and after an estimation cycle due to reduced SOC

The impedance measurement is done by taking the quotient of the amplitudes of the induced DC bus voltage and excited DC bus current wave form. Using the simplified battery model depicted in figure 2.2, this quotient would roughly reflect the electrolyte resistance when measured at a high enough frequency. The frequency needed for this to be true is not easily calculated or derived from literature, mostly because of variances between batteries. Instead, the highest possible frequency with respect to the minimum amount of harmonics is used. Since estimation is done by linear regression, the regression model is more important than the actual nature of the measurement.

The preload was implemented to lower short term capacitive effects of the battery and also to get the terminal voltage at a constant and known load. It was observed during early algorithm prototyping that if the terminal voltage was given time to recover, the measurements would suggest a high SOC. In the same manner, if a measurement was performed close to the end of a load cycle, the measurements suggest a low SOC. By using a DC preload that transitions into an impedance measurement, results became more consistent.

Parameters that are used for SOC estimation are terminal voltage slope at start of preload, terminal voltage at end of preload, measured phase difference between current and voltage peaks, and lastly the Ohmic impedance. In [15], phase angle was found to vary with SOC, making it an interesting parameter for the estimation. All measurements are done using only the motor controller without external hardware, although as previously mentioned, external hardware was used for verification of function. Data was collected using DriveTool and processed in Microsoft Excel for ease of visualization.

Early prototypes used a simpler linear model of the terminal voltage, measured Ohmic impedance and was somewhat successful in estimating the SOC. To expand insight and improve estimation, the model was extended to include said parameters.

Model parameterization

Model parameters $p_1 \dots p_8$ were determined using Gauss-Jordan elimination implemented in Excel. With our measurements vector $M(m \times 8)$ consisting of m measurements taken at several intervals throughout the SOC and our known SOC vector $S(m \times 1)$ (determined by density measurements at the time of each measurement), we can solve for the optimal $P(8 \times 1)$ parameter vector:

$$\begin{aligned} MP &= S \\ M^T MP &= M^T S \end{aligned} \tag{4.8}$$

which when solved using Gauss-Jordan elimination yields

$$\begin{bmatrix} 1 & 0 & 0 & \cdots & 0 \\ 0 & 1 & 0 & \cdots & 0 \\ 0 & 0 & 1 & \cdots & 0 \\ \vdots & \vdots & \vdots & \ddots & \vdots \\ 0 & 0 & 0 & \cdots & 1 \end{bmatrix} \begin{bmatrix} p_1 \\ p_2 \\ \vdots \\ \vdots \\ p_8 \end{bmatrix} = (M^T M)^{-1} M^T S \tag{4.9}$$

4.4.1 Final model for estimation

The final model is a segmented regression model consisting of one 1^{st} order V_t polynomial and three 2^{nd} order polynomials in $\dot{V}_t$, R_i and ϕ, all four with shared constant coefficient.

Notations:

- $\mathrm{V_t}$ Battery terminal voltage, in Volts.
- $\dot{\mathrm{V}}_\mathrm{t}$ $\frac{d}{dt}\mathrm{V_t}$, in V/s.
- $\mathrm{R_i}$ Measured Ohmic impedance, in Ohms.
- ϕ Phase offset between current and voltage waves, in system ticks.

A matrix form representation of one of the two model parts looks as follows:

$$SOC = \begin{bmatrix} p_1 & p_2 & p_3 & p_4 & p_5 & p_6 & p_7 & p_8 \end{bmatrix} \begin{bmatrix} V_t \\ \dot{V}_t \\ \dot{V}_t^2 \\ R_i \\ R_i^2 \\ \phi \\ \phi^2 \\ 1 \end{bmatrix} \tag{4.10}$$

and as a linear combination:

$$SOC = p_1 V_t + p_2 \dot{V}_t + p_3 \dot{V}_t^2 + p_4 R_i + p_5 R_i^2 + p_6 \phi + p_7 \phi^2 + p_8 \tag{4.11}$$

The model has been divided into two segments separated by a boundary terminal voltage V_{tb}. The segment responsible for estimation above V_{tb} is designed to cope with the effects of slight overcharge and the *coup de fouet*. The other segment is responsible for the fairly quadratic remainder of the solution space. Both models are functionally identical, but the parameters $p_1 \ldots p_8$ differs slightly. To smoothen the transition between model segments, each segment was parameterized with measurements slightly above and below V_{tb}, respectively.

Chapter 5

Software implementation

5.1 Design overview

The software is for the most part organized in a hierarchy of different state machines with varying purposes:

- An external state machine tracks the overall state of the function by looking at a number of variables, such as the status of the power stage and SOC estimation request flag.
- Inside the measurement state of the external state machine is the internal measurement state machine. It tracks the progression of the estimation sequence by a timer variable and two Kalman filter flags.
- Measurements of the various impedance quantities are done using dual state machines that track sine wave forms.

Figure 5.1 and the associated text explains the outline of the application flow.

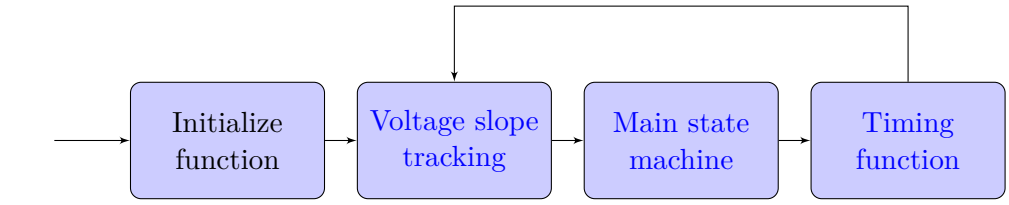

(a) Estimation function overview

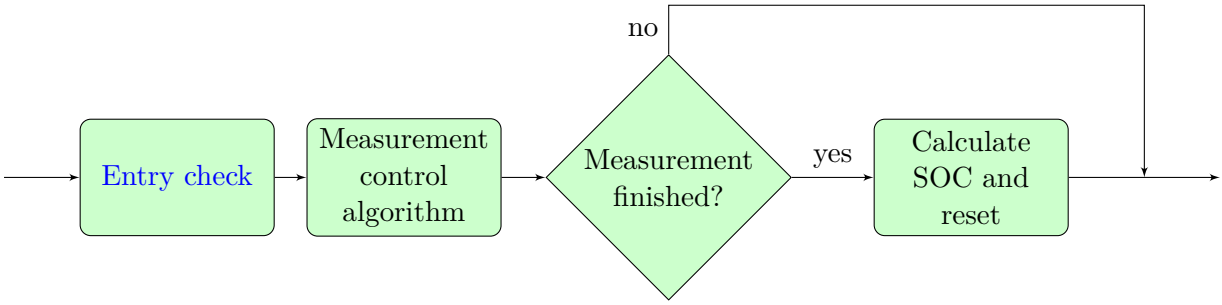

(b) Detail: Main state machine

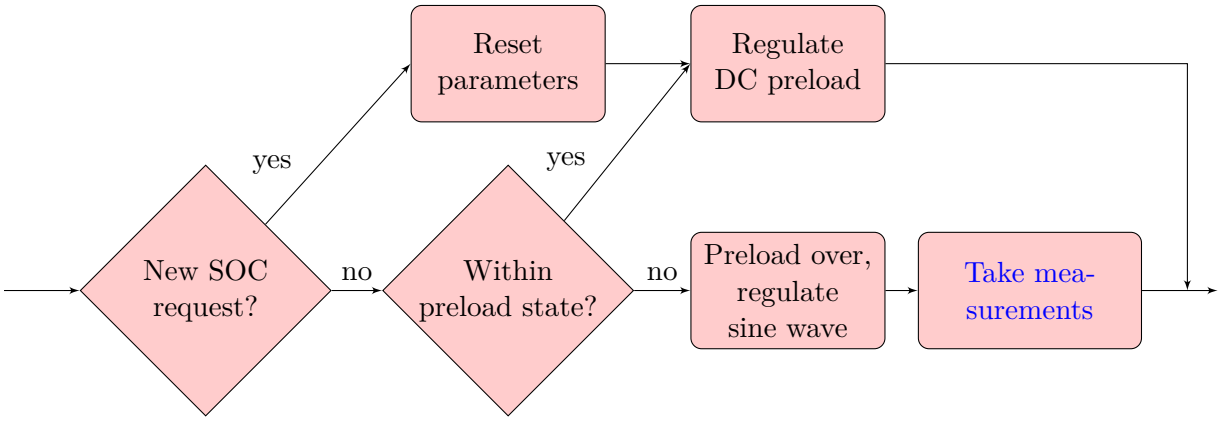

(c) Detail: Measurement control algorithm

Figure 5.1: Software outline

5.2 Voltage slope tracking

To measure the terminal voltage slope with respect to time, a filtered internal voltage measurement was read by the estimation function. To cope with the remaining noise, a piecewise mean value algorithm was applied. It was implemented as a circular two-tier buffer. The lower buffer calculates the mean voltage over 10 ms and stores the value in the upper buffer. When the upper buffer is full, a mean slope is calculated by the difference between the head and tail of the upper circular buffer.

5.3 Main state machine

The main state machine of the function keeps track of the measurement process, and uses various variables to decide what action to take. Initially, a timer variable keeps track of the amount of time spent preloading the battery with a direct current. Afterwards, action taken is dependent on the number of measurements taken while regulating the sine wave.

5.4 Timing function

A simple timing function was implemented to track algorithm performance using system ticks. Each pass through the function is timed and saved as an external parameter that can be plotted using DriveTool.

5.5 Entry check

For access control to the measurement algorithm, i.e. when to do measurements and when to stop et cetera, a bouncer semantic was applied. If the function had gotten an external SOC request – or is already processing an old request – program flow would enter the measurement algorithm. The bouncer would also check if the active request is new in which case it would have to reset the measurement parameters, and if the motor controller power stage is enabled.

5.6 Taking measurements

To simplify program flow and increase code readability, all measurements were done simply by feeding the momentary terminal voltage and DC bus current to its respective state machine – not to be confused with the encompassing main state machine. This state machine type is designed to track sine wave forms. Peaks and valleys are tracked by slope sign transitions and the potential difference between peaks and valleys is stored for both DC bus current and terminal voltage.

A shared variable was introduced to the two state machines that allowed for simple communication. Using this variable, the estimation function was able to measure the phase difference between current and voltage in function ticks.

Several filters were used to reduce high frequency noise and DC components of measurements. Low pass filters used were discretized first-order RC filter circuits. Bandpass filters were implemented using double low pass filters as

$$y_{filtered} = F_1(y) - F_2(y) \tag{5.1}$$

where F_1 and F_2 denotes a low pass filter output function with associated cut off frequencies f_1 and f_2, and where

$$f_1 > f_2 \tag{5.2}$$

Resulting in the output signal with frequencies

$$f_1 < f_{y_{filtered}} < f_2 \tag{5.3}$$

In reality – since the filters are first-order – there will still exist signals with frequencies lower than f_1 and higher than f_2, although with dampening proportional to the distance to their respective cut-off frequency.

To filter the measured excited DC bus voltage and current potential differences, a mean value function working on a circular buffer was combined with a one dimensional Kalman filter with sliding measurement error covariance, R. During the measuring process, R is stepped up from a low initial value to a relatively high end value. This way the filter converges faster than if a fixed high R is used, and noise is progressively smoothened out.

Chapter 6

Results

6.1 Estimation

At 32-bit shift resolution, the composite model shows a mean SOC error of +0.5 percentage points, with a standard deviation of 1.048. The estimation error was measured to be in the interval of +0.5 ±2.7 percentage points (P = 0.99) when applied to the data used for regression, affirming the model design. See figure 6.1.

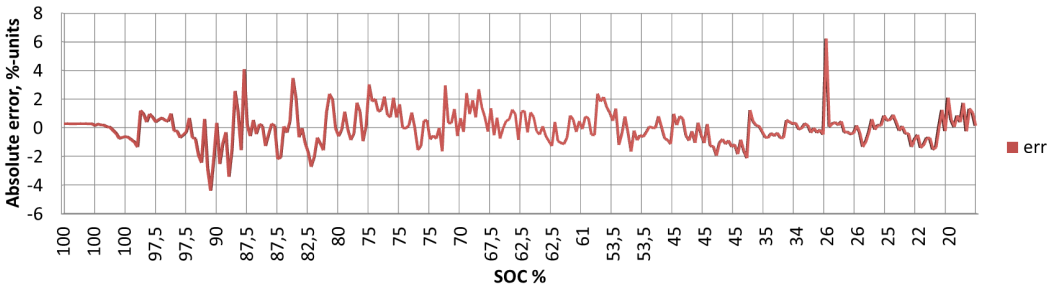

Figure 6.1: Absolute error over a discharge cycle using regression data.

After model implementation, the algorithm was tested ”live” in the motor controller on a separate occasion. The results showed an estimation error of -3.7 ±4.8 percentage points (P = 0.99). The difference between actual and measured SOC can be seen in figure 6.2. The model still produces a fairly linear relationship with the actual SOC as can also be seen in figure 6.3, which also shows low precision in high SOC.

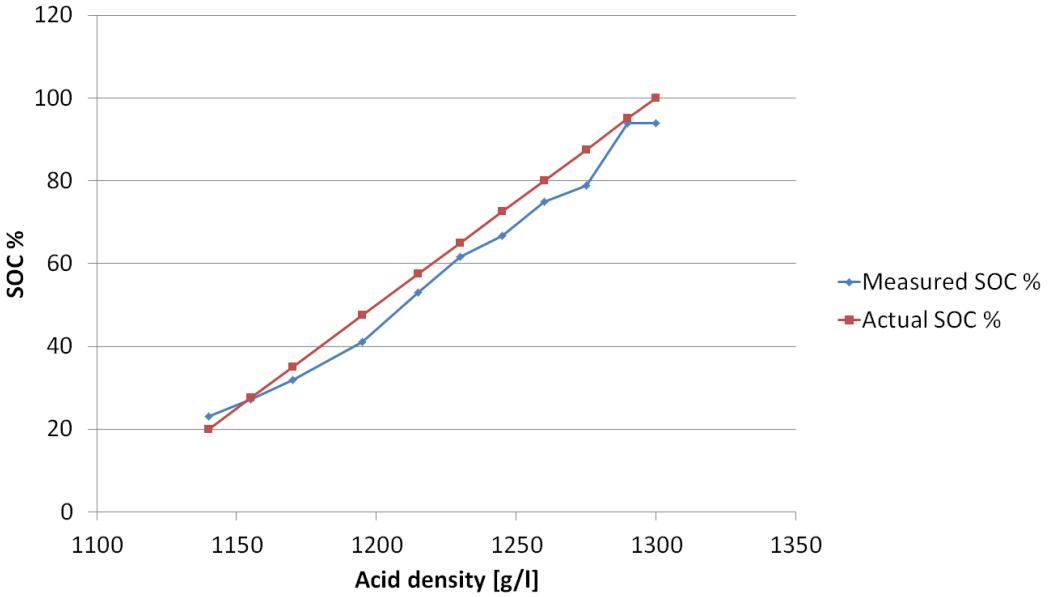

Figure 6.2: 15-point average measured SOC versus actual SOC from acid density.

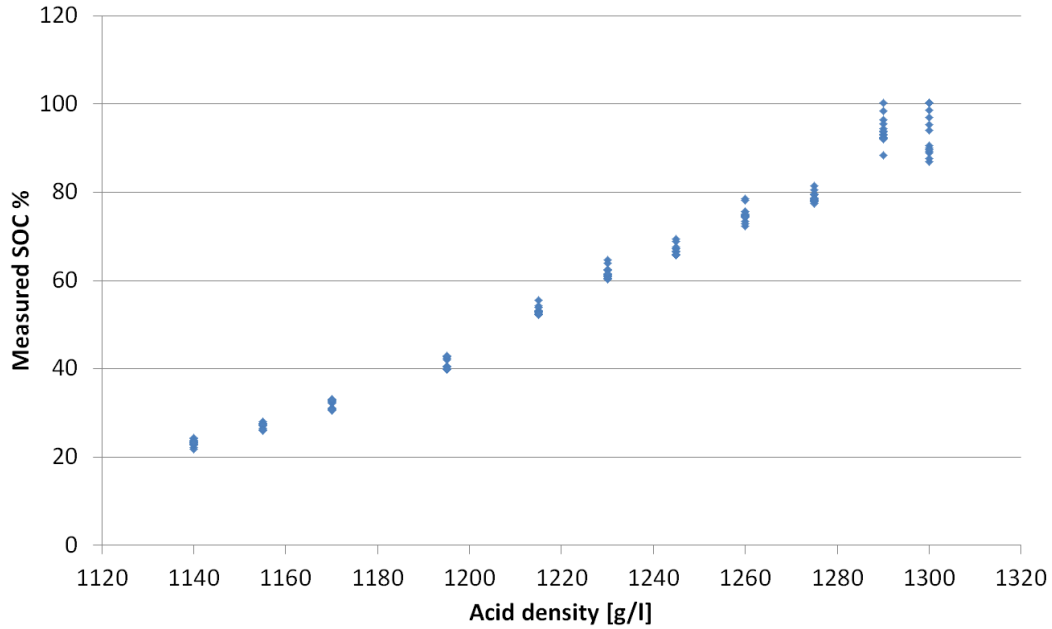

Figure 6.3: Distribution of measurements by acid density.

6.2 Algorithm performance

The implemented algorithm was evaluated using the timer function described in section 5.4. In figure 6.4 the number of system ticks per function run is shown versus the number of function runs per SOC estimation sequence. The red line when high represents a period of active SOC request.

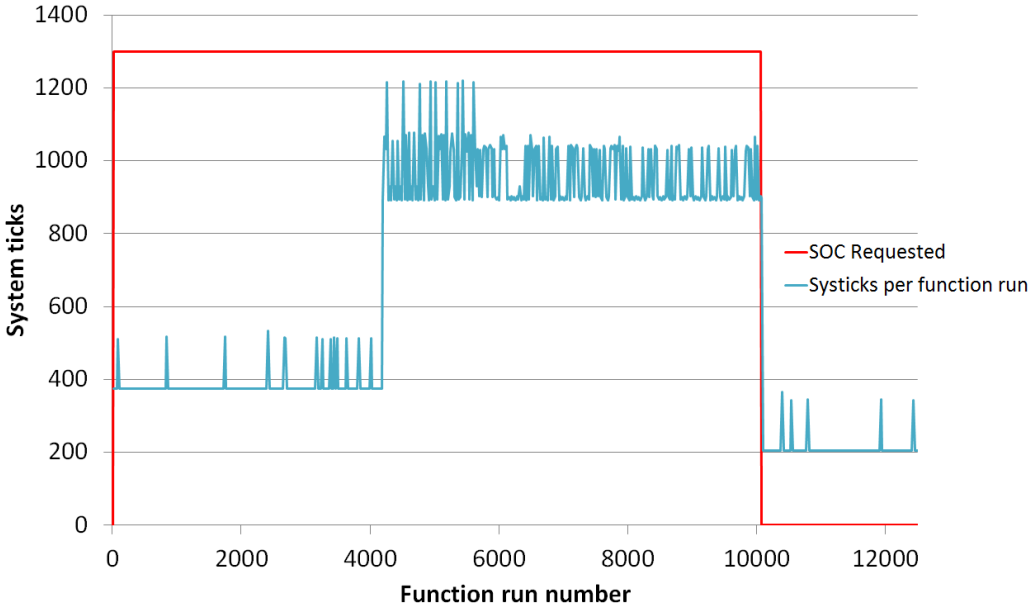

Figure 6.4: System ticks per function run and total number of function runs.

It is shown that the number of system ticks per function run has a maximum of roughly 1200 ticks, which translates to $\frac{1200}{72MHz} \approx 16.7\mu s$. Since the function frequency is 4 kHz this makes up $\frac{16.7 \cdot 10^{-6}}{1/4000} \approx 6.7\%$ of the entire period. The number of function runs per estimation sequence is slightly above 10000, which is $\approx \frac{10000}{4000} = 2.5s$.

Chapter 7

Analysis and conclusion

7.1 Analysis

A deviant result was observed when the algorithm was implemented in the motor controller as opposed to the results from the development of the regression model. This is most probably ascribed to the fact that the measurements took place on different occasions, during the second of which the ambient temperature was noticeably lower compared to the first. This caused a measurable thickening of the electrolyte, which in turn seemed to increase internal battery resistance and phase shift. This strongly suggests – not surprisingly – that the proposed model has a slight temperature dependency, but still keeps an accuracy within the set limits of the hypothesis, especially given that the exploration of temperature dimensionality was outside the scope of the thesis work.

It is worth noting that while the battery SOC estimation was offset negatively because of lower electrolyte temperature, the lower temperature also decreases available capacity. This effectively balances the error in SOC estimation, but to what extent is not explored. Intuitively, if the battery is fully charged but with 10% reduced capacity because of low ambient temperature, it can also be viewed as being at 90% SOC with respect to baseline capacity. Recalling equation 4.1 and using the battery data sheet, we see that a 10 degree Celsius change in temperature corresponds to a change in percentage units of 3.5, which may explain the -3.7 percentage units offset described in the results section 6.1 and graphically in figure 6.2.

The temperature aspect could also help explain the estimation improvement near the end of the discharge cycle. In the figure, end of discharge corresponds to the acid density interval of roughly 1140–1180. The electrolyte density has already been established to be linear in time at a fixed discharge current and temperature. Making the assumption that electrolyte resistance is moderately proportional to the density of charge transfer ions and therefore increasing in a linear fashion during discharge, the power dissipated in the electrolyte would also be linearly increasing. Integrating over time, the total amount of energy transferred to the electrolyte would then increase quadratically. As the temperature increases quadratically, so

would the estimated SOC value due to faster electrolyte convection. In figure 6.2, estimated SOC can be seen increasing somewhat quadratically towards the end. Therefore, a possible explanation is that the electrolyte temperature passed the parameterization temperature at a density of slightly below 1160 g/l.

7.2 Conclusion

Considering the constraints of the thesis work, the algorithm has managed to perform adequately under controlled circumstances. Even without taking the possibility of temperature self-balancing into account, the algorithm performs within the limits of the ± 10 percentage units set beforehand. This has been achieved using no external sensors and designed and implemented in a way that fits in the "ambient" thread environment in the processor. With this, the proposed hypothesis can be accepted.

Chapter 8

Recommendations and future work

8.1 Recommendations

For anyone who is looking to engage in researching batteries – regardless of technology – one main consideration quickly springs to mind: never underestimate the non-linearity of batteries. The few parameters and attributes that are vaguely linear tend to need a very long resting period to be valid for SOC estimation. The electrochemical processes involved in battery operation cannot be approximated to simpler models without a significant loss of accuracy.

It is also a strong recommendation to always consider the temperature dependency when working on battery analysis. Different applications are sure to need different approaches for battery state-of-function estimation, and temperature dependency is present in more or less all aspects of estimation. Depending on the application at hand, make sure to try to find and use parameters that exhibit the least temperature dependency.

8.2 Future Work

8.2.1 Temperature dependency

The most obvious aspect to consider in future work building on this model would be to include a dimension of electrolyte temperature. It would be interesting to see if temperature affects inter-parameter relationships, and therefore would make the model able to account for temperature without needing an actual measurement. The laboratory setup would have to be extended with an insulated and temperature controlled housing for the battery, and sufficient time for temperature stabilization. A concern with that setup is that the electrolyte resistance would cause internal heating of the battery, and thereby disturb measurements if not accounted for.

Another temperature aspect that has been briefly touched on earlier in the report is the estimation error due to altered ambient temperature. In a colder laboratory environment, SOC is estimated to be lower than in a relatively warmer

environment. It would be of interest to investigate how much this actually reflects a lowered capacity instead of being an error in estimation. This would demand a controlled environment for the battery, electrolyte temperature sensing and temperature compensation of state-of-charge calculations from acid density.

8.2.2 Non-linear model

To try to model the non-linear behavior of the battery, the now linear model could be extended to non-linearity. Considering the simplicity of the underlying battery model and noisy measurements, it would most likely require a large amount of work, and the net gain in accuracy after including time spent in development might be less than satisfactory.

8.2.3 Square wave generation

One disadvantage with exciting a sine wave for measurements of Ohmic resistance is that the resolution of the wave form decreases quickly at higher frequencies than 200 Hz. To cope with the resolution shift, a solution could be to change wave form to a square wave. Current regulation would be much simpler and potential harmonics could be filtered out or taken into account when measuring the voltage response. The square wave frequency would still be limited by the rise time of the current regulator and by the maximum current amplitude that can be excited. A higher current amplitude excites a higher amplitude in the voltage response , making it less sensitive to noise.

8.2.4 Frequency sweeping

With or without the implementation of the square wave form, a frequency sweep could improve estimation accuracy by providing a much larger data set. Complexity and calculation times would increase with the number of frequencies to sweep, which is another argument for square wave implementation because of the more lightweight regulation.

There are however some concerns to take into account. During the thesis work, it was found that long discharge times (more than a few seconds) would affect measurements more than what could be seen in the change in SOC in the same time. It might be that a sequential sweep could generate overly skeptic readings in the last few frequencies. Although, to mitigate this risk it could simply be a matter of taking those effects into account. On the other hand, the whole estimation model would change drastically with sweep timing changes.

8.2.5 Noise reduction

Avoiding prolonged discharge is advantageous for several reasons. Partly for reasons mentioned in the previous paragraph, but also for the fact that the currents drawn from the battery while performing estimation are large, in the order of 50 to 100

A. In the case of single frequency measurements, the effect might be negligible but in case of a frequency sweep the current could very well actually affect the SOC. Also, long measurement periods could mean that the SOC estimation might not have time to finish before the vehicle starts moving again.

8.2.6 Static slope point of measurement

If the voltage tracking functionality were to be improved, the dimension of voltage slope could be dropped from the model. By setting a threshold value for the slope, measurements would be performed at a near static slope value. This simplifies the model and opens up for other possible model parameters. For example, measuring the difference in terminal voltage before and at the end of the preload period. With a static slope point, it would also be possible to develop faster and simpler algorithms that are less accurate but more easily implemented.

8.2.7 Coulomb counter

If the system has an accurate DC bus current sensor, it would be simple to implement a Coulomb counter in parallel with any kind of absolute SOC value estimator. This would make the system capable of estimating not only SOC but also the SOH of the battery by comparing the change in absolute value to the outgoing Ampere hours.

8.2.8 Flow optimization

The processor load footprint could be reduced to close-to-none during vehicle operations with code optimization and a slight program flow redesign. At the moment, terminal voltage tracking is performed continuously instead of only when needed. The need for tracking would only arise when the vehicle comes to a stop and the time since the last estimation has exceeded an arbitrary threshold.

Bibliography

[1] K. Bullock. Lead/acid batteries, 1994.

[2] C. Glaize and S. Genies. *Operation of lead-acid batteries*. 2012.

[3] D. Schulte et al. Stratifiability index. *Journal of Power Sources 269*, 2014.

[4] H. Catherino et al. Sulfation in lead-acid batteries. *Journal of Power Sources 129*, 2004.

[5] Dennis Doerffel and Suleiman Abu Sharkh. A critical review of using the peukert equation for determining the remaining capacity of lead-acid and lithium-ion batteries. *Journal of Power Sources 155*, 2006.

[6] BaSyTec. The influence of temperature on the operation of batteries and other electrochemical energy storage systems. http://www.basytec.de/Literatur/temperature/DE_2002.htm, July 2014.

[7] Battery University. How heat and loading affect battery life. http://batteryuniversity.com/learn/article/how_heat_and_harsh_loading_reduces_battery_life, July 2014.

[8] Enersys-Hawker. Hawker perfect plus. http://www.enersys-hawker.com/, 2014.

[9] NorFalco. Densities of sulfuric acid in kg/liter. http://www.norfalco.com/EN/ProductsServices/Documents/3, 2014.

[10] M. Perrin and A. Delaille. *Coup de fouet*. 2009.

[11] P. Pascoe and A. Anbuky. The behaviour of the coup de fouet of valve-regulated lead-acid batteries. *Journal of Power Sources 111*, 2002.

[12] Ahmed Fasih. Modeling and fault diagnosis of automotive lead-acid batteries, 2006.

[13] Gamry Instruments. Basics of electrochemical impedance spectroscopy. https://www.gamry.com/application-notes/basics-of-electrochemical-impedance-spectroscopy/, 2014.

[14] M. Piller, S. Perrin and A. Jossen. Methods for state-of-charge determination and their applications. *Journal of Power Sources 96*, 2001.

[15] S. Rodriguez et al. A review of state-of-charge indication of batteries by means of a.c. impedance measurements. *Journal of Power Sources 87*, 2000.

[16] P. Roberge and E. Halliop. Non-destructive characterization of sealed lead/acid celles with electrochemical impedance spectroscopy. *Journal of Power Sources 32*, 1990.

[17] F. Huet. A review of impedance measurements for determination of the state-of-charge or state-of-health of secondary batteries. *Journal of Power Sources 70*, 1998.

[18] A. Jossen et al. State-of-charge determination for lead-acid batteries in pv-applications. *Proceedings of the 16th European Photovoltaic Solar Energy Conference*, 2000.

[19] Dal Y. Ohm. Dynamic model of induction motors for vector control.

[20] IAR Systems. Iar embedded workbench. http://www.iar.com/Products/IAR-Embedded-Workbench/Technology/Components/, 2014.